Wave Energy Harnessing in Shallow Water through Oscillating Bodies

Marco Negri * and **Stefano Malavasi**

Department of Civil and Environmental Engineering, Politecnico di Milano, 20133 Milan, Italy;
stefano.malavasi@polimi.it

* Correspondence: marco.negri@polimi.it; Tel.: +39-02-2399-6260

check for
updates

Abstract: This paper deals with wave energy conversion in shallow water, analyzing the performance of two different oscillating-body systems. The first one is a heaving float, which is a system known in the literature. The second one is obtained by coupling the heaving float with a surging paddle. In order to check the different behaviors of the multibody system and the single-body heaving float, physical models of the two systems have been tested in a wave flume, by placing them at various water depths along a sloping bottom. The systems have been tested with monochromatic waves. For each water depth, several tests have been performed varying the geometrical and mechanical parameters of the two systems, in order to find their best configurations. It has been found that the multibody system is more energetic when the float and the paddle are close to each other. Capture width ratio has been found to significantly vary with water depth for both systems: in particular, capture width ratio of the heaving float (also within the multibody system) increases as water depth increases, while capture width ratio of the paddle (within the multibody system) increases as water depth decreases. At the end, the capture width ratio of the multibody system is almost always higher than that of the heaving float, and it increases as water depth increases on average; however, the multibody advantage over single body is significant for water depth less than the characteristic dimension of the system, and decreases as water depth increases.

Keywords: wave power; wave energy converter; heave; surge; shallow water; capture width ratio

1. Introduction

Renewable energies are increasingly becoming a main topic of interest among scientists due to the need for sustainable development, the increasing energy world request and the expected depletion of fossil fuels. Among the third generation renewable energies, wave energy is one of the most promising. Since the second half of the last century many attempts to harvest wave energy have been made, but no device has yet to reach full commercial production, while several have achieved the prototype stage, e.g., the Wavestar (Wave Star Energy A/S, Brøndby, Denmark www.wavestarenergy.com), the Seabased AB (Seabased industry AB, Lysekil, Sweden www.seabased.com), the Ceto (Carnegie Wave Energy, Belmont, Australia https://www.carnegiece.com/wave/), and many other important ones like the Oyster (Aquamarine Power, Edinburgh, UK) and the Pelamis (Pelamis Wave Power, Edinburgh, UK) whose further development ceased.

Wave energy converters (WECs) are very various and can be classified according different criteria: a common subdivision of WECs is according to their working principle [1], which are oscillating water column (OWC), oscillating body, overtopping. Other important classifications are according to location (offshore, nearshore, shoreline) and directional characteristic with respect to the oncoming wave (point absorber, attenuator, terminator) [2]. Reviews [1,2] are extensive works including the characterization

of wave energy resource and the compendium of WEC technologies. A more recent review of wave energy technology can be found in reference [3].

Wave energy exploitation still has high investment costs, therefore, in the last ten years, hybrid solutions with other renewable sources like wind and solar have been proposed; this allows limiting installation costs and achieve a more regular energy production (see for example [4]). On the other hand, wave energy exploitation is economically advantageous for islands and remote coastal areas, where the electric grid is absent and fuel supply is difficult; reviews of wave energy and hybrid (wave, tidal, wind, solar) technologies suitable for these areas can be found respectively in references [5,6].

One of the principal issues with WECs is the ratio between energy production and costs. Offshore system (water depth >50 m) seems to be preferable due to the greater energy amount of the open sea waves, while shoreline systems usually have a lower energy availability, due to energy dissipation caused by the travelling of the waves in shallow waters. Exceptions to this generalization are those particular places (promontories or isles), called hot spots, where, for refraction and diffraction effects, a concentration of wave energy can be found [7]. On the other hand, offshore WEC have higher costs of installation, maintenance and connection to the electrical grid compared to shoreline system, due to obvious reasons of shore proximity.

The reduction of wave energy from offshore to nearshore is better explained in reference [7]: If it is true that the gross wave energy significantly reduces, on the contrary the exploitable wave energy can be quite similar. The exploitable wave energy is directional-resolved and does not include the sea storms. Folley and Whittaker [7] found, analyzing two sea sites in North Atlantic coast of Scotland, that the exploitable wave energy is reduced only by 7% and 22% from offshore to nearshore.

In the same work, it is also shown that the bottom slope influences wave energy dissipation, and that a steeper bottom causes less energy dissipation by bottom friction, as waves travel a shorter distance in shallow depths to reach the nearshore zone. In reference [8], numerical simulations of wave propagation along a sloping beach are performed, considering various wave heights and periods, and beach slopes. It is shown that, for example, a wave with significant wave height H_{m0} = 4 m loses only about 20% of its power when travelling from deep water to a depth of 10 m, on a 1:100 sloping beach. Thanks to these considerations we can understand why nearshore sites have been revalued for wave energy harvesting, and several studies are being made to estimate the energy availability in many nearshore places, e.g., references [9–11]. Indeed, wave energy dissipation in the nearshore zone depends on so many factors, like wave properties, angle of propagation, bottom slope and bottom roughness [12] so that wave energy availability may significantly vary along the coast, and each site should be individually characterized.

Besides water depth, also local irregularities of the seabed affect the WEC behavior, due to their influence on the wave propagation (see for example [13]). Therefore, localizing a suitable position for a WEC is a matter of fundamental importance; in reference [14], the numerical simulation of various well-known WECs in several points of the Portuguese nearshore also showed that the local energy availability is not the only factor affecting the WEC energy production.

It is known that water particle trajectories in shallow water waves are different than the ones in deep water; the elliptic shape of the trajectories causes nearshore waves to have a higher surge force than offshore waves; in reference [15] it is shown that the capture width ratio (CWR) of a surging oscillating flap in 10 m water depth can be more than double than in deep water. For the Oyster, a bottom-hinged pitching-surging flap of 12 m of width installed in 12 m water depth (the flap was surface-piercing), CWR up to 70% was evaluated [16].

Nearshore sites are still good places for heave oscillating bodies, as evidenced by the Danish Wavestar prototype located at Hanstholm, which is placed in a water depth of about 6 m. The Wavestar prototype is composed of two hemispherical pitching-heaving floats of 5 m diameter, each of which is supported by an arm that is pivoted to a fixed structure above water [17]. A peculiarity of Wavestar is that the floats are aligned along the wave propagation direction, in order to supply a continuous force to the power take-off (PTO) system as wave travels through the floats.

In this work, we have compared the performances of two similar WECs in shallow water placed on a sloping bottom, in water depths of the order of the WEC diameter. One is a pitching-heaving float, similar to the Wavestar system [17], except for the fact that the arm that supports the float is aligned along wave propagation direction (hereinafter we will refer to this system as "float-only"). The heaving float is the most basic oscillating-body WEC (see reference [1] for some examples). Generally, the heaving float is studied in deep water (>40 m) and, to the author knowledge, there is not a specific study on the influence of water depth; in this work, we investigate the behavior of a heaving float in water depth ranging between 0.6 and 2 float diameters.

The other WEC tested in this work is the Energy Double System (EDS), a multibody system that consists of the pitching-heaving float plus a pitching-surging paddle (Figure 1). By removing the paddle from EDS, the float-only system is obtained. In the perspective of an array arrangement, the EDS modules would be aligned parallel to wave front, unlike Wavestar system whose modules are orthogonal to the wave front. In the EDS system, the paddle is supported by an arm hinged on the main arm. The original idea behind this WEC is to harness both heave and surge wave forces, in order to ensure a large exploitation of the wave resource and to obtain a good flexibility toward different sea conditions.

Usually, multibody WECs are composed by two bodies that exploit the same wave force (typically heave force, see reference [1]); the advantage of these WECs is that the PTO can use the relative motion between the two bodies instead of reacting against a fixed point on the seabed or on the ground. In this way, there is the additional benefit of avoiding the practical issues of foundation construction. Examples of heaving two-bodies WECs are [18,19].

The peculiarity of EDS is that the two bodies composing it exploit different wave forces, heave and surge. In this work, we analyze the advantages of coupling a heaving float and a surging paddle in a sole WEC, and we verify whether it is energetically advantageous compared to the heaving float, given that the paddle would be a relatively simple addition to the latter.

EDS has some important advantages, such the relatively low costs due to its nearshore positioning, the possibility to be attached to existing structures, and the modularity. These characteristics make EDS particularly suitable for ports, where piers and breakwaters would provide a base to attach the system or lay the foundation of EDS. The energy produced could be directly utilized for port operations and for providing electrical power to the ships while stationary (cold ironing), increasing the environmental sustainability of the port. The natural variation during the year of the available wave energy fits with the activity of the boats inside the port: most of the yearly wave energy comes from autumn to spring, and this is also when more energy is required because of the dry berthing and maintenance of the boats. In summer, when the available wave energy and the energy demand for boat management are smaller, EDS could even be stored out of water, especially if it impedes the boat traffic through the port, which is greater in the hot season.
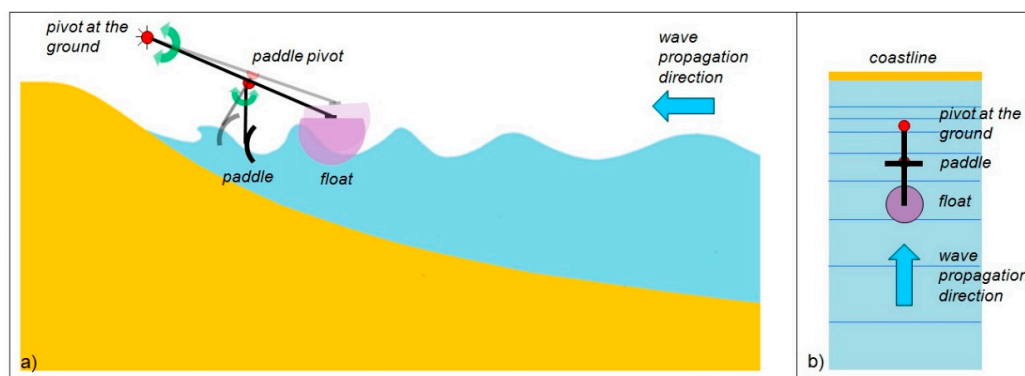

Figure 1. EDS concept. (**a**) side view; (**b**) top view.

EDS is a point absorber/terminator WEC: it is designed for harnessing waves shortly before they break, when their energy content is still relevant. The ideal depth is 3–10 m, depending on

the sea spectrum and site characteristics. Both paddle and float are "light systems", as they are not resonant with waves. Paddle predominately works in the direction of wave propagation, pushed by the drag force originated by the mass transport of waves just before they break. A paddle of this type is potentially more energetic in shallow water than in deep water. Hazlett et al. [20] tested a similar paddle in deep water: it was a surface-piercing or half-immersed paddle that had the possibility to translate along the wave propagation direction, pushed by the waves. They measured a maximum CWR of 15% when the paddle was artificially driven so that it stayed on the wave crest; otherwise, CWR did not exceed 5%. A first scale model of EDS was studied in reference [21], providing early indications about system potentiality. In this work the EDS model has been significantly improved to make it more realistic and the influence of several parameters on system performance has been deeply investigated.

The first part of this work deals with the description of the experimental model. Then, the results of the experimental tests on the float-only system and on EDS are presented. Finally, the performances of the two systems are discussed in more details, and they are compared with the ones of the the Wavestar lab model [22].

2. Experimental Setup and Method

This part is subdivided in three sections: the first one describes the laboratory model of the EDS, the second one describes the data processing calculation of the power absorbed by the EDS model, and the third one describes the laboratory waves used in the experiments.

2.1. EDS Scale Model

The laboratory model of EDS is shown in Figure 2. It has been realized at 1:25 scale of the project prototype, and it is composed of a main arm $\overline{OA}$, which supports the float and which is pivoted at O above the water surface. Another arm $\overline{CE}$ supports the paddle and it is pivoted in point C on the main arm, between the pivot O and the float. The two degrees of freedom of the system are θ_1 and θ_2, angles of rotation of the float around O pivot, and of the paddle around C pivot, respectively. θ_1 and θ_2 are both absolute coordinates: they express rotations around the equilibrium position of the main arm and paddle arm respectively.

The float is composed by a hemispherical part at the bottom with radius 0.107 m and height 0.075 m, and a cylindrical upper part with diameter 0.204 m and height 0.062 m. Total height of the float is 0.137 m. The paddle has a cylindrical shape with radius 0.104 m and a chord of 0.12 m. The paddle width is 0.204 m. Main characteristics of the model and their uncertainties are reported in Table 1. In order to support the float PTO, the main arm extends on the left hand side of O pivot up to point B. Paddle PTO is placed between the paddle arm (point D) and the main arm (point F). Both PTOs are heaving discs in not-pressurized oil (density 878 kg/mc, dynamic viscosity 0.12 Pa·s at 20°), connected through leverages to the main arm or to the paddle arm. The float-only system is obtained by removing the paddle apparatus, which consists of the paddle, its arm ($\overline{CE}$) and its PTO with the leverages ($\overline{DF}$); in this way the system turns into a one-degree-of-freedom system and it becomes similar to the Wavestar model studied in reference [22]. With respect to the EDS model of the previous work [21], the main improvements made in this work are:

(1)　Float geometry: the shape of the float has been improved, by further rounding the basis of the float, making it more hydrodynamic. Moreover, the new float is shorter, the cylindrical part is shorter and the spherical part is taller. This make the new float quite similar to the one used in [22].

(2)　Inertia: also related to the float geometry, the inertia of the new model is lower. This make the new model more realistic.

(3)　Paddle PTO: the new model has a dissipative system for measuring energy absorbed by the paddle, while in the previous model the absorbed energy was estimated by the elongation of a spring connected to the paddle. That was a conservative system, hence the absorbed energy could not be accurately measured.
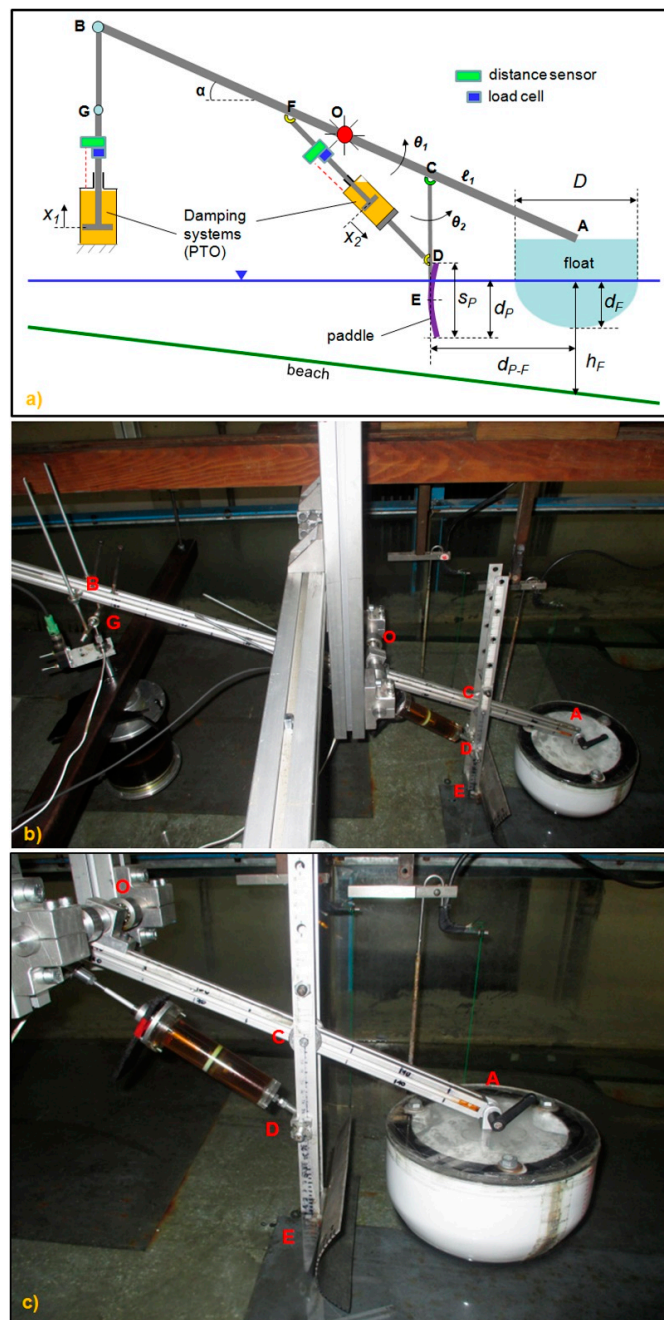
Figure 2. (**a**) EDS scheme model; (**b**) EDS lab model; (**c**) EDS lab model, particular.

Table 1. Characteristics of the EDS laboratory model.

Characteristic	Symbol	Value
Float arm length	l_1 [m]	0.4 ± 0.0005
Main arm inclination	α [°]	25 ± 1
Paddle height	s_P [m]	0.12 ± 0.0005
Paddle draft	d_P [m]	0.09 ± 0.001
Float draft	d_F [m]	0.06 ± 0.001
Diameter of the float, paddle width	D [m]	0.204 ± 0.0005
Moment of inertia	I [kg m^2]	0.45 ± 0.02
Hydrostatic stiffness of float	k [Nm/rad]	36 ± 1
Natural period of the float-only system	T_N [s]	0.84 ± 0.01

Figure 3 is a schematic of the PTO systems of float and paddle. The float damper is a single heaving disc, supported by a stem that can slide through bearings. The bearings are fixed at the cylinder, which is fixed to the ground. The amount of damping was changed by varying the diameter of the heaving disc. The diameters of the discs used were 93, 96, 99, 100 mm; the internal diameter of the cylinder was 104.8 mm.
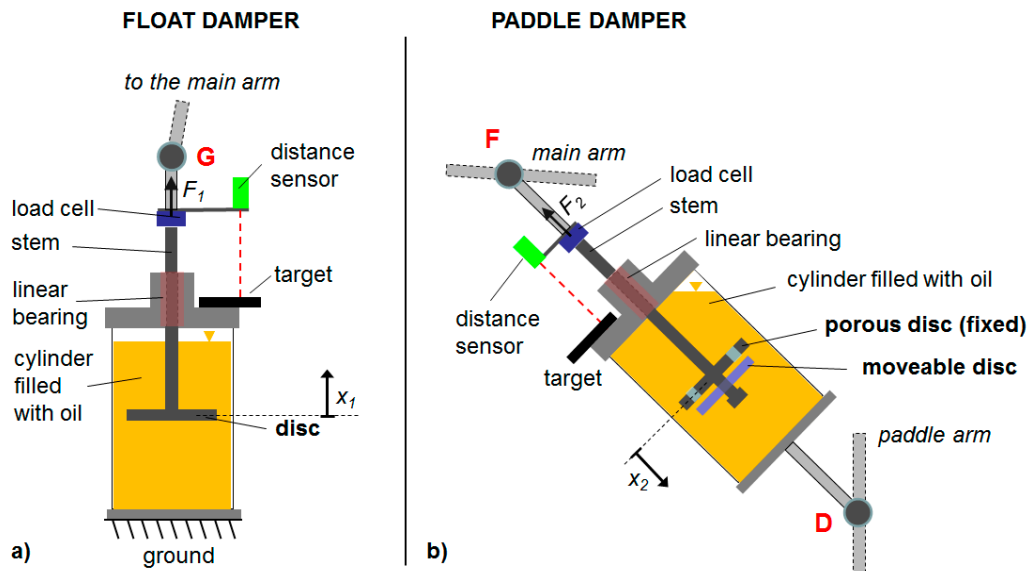

Figure 3. PTO of float (**a**) and paddle (**b**).

The paddle damper is similar, except for two characteristics. The first one is that the stem supports two heaving discs, a porous one fixed on the stem, and another one that can slide along the stem for a short distance. This system allows for a different amount of damping in the two ways of motion of the stem. Depending on the way of motion, the discs are attached together or detached and the holes of the fixed disc are closed or freed. The diameter of the fixed disc is 23 mm, with eight holes of 3 mm diameter; the diameter of the cylinder is 24 mm. The other difference between the float and paddle PTO is that the latter reacts against the main arm in point F and not against the ground. Point F is at the left hand side of point O (see Figure 3) and the length of segment OF (see Figure 2a) is 0.130 ± 0.005 m. A sensor distance and a load cell were placed on each PTO system, in order to measure the relative motion $x(t)$ between the disc and the cylinder and the force exerted on the disc.

2.2. Measurement Method

The distance sensors measure the relative position x_1 and x_2 between the stem and the cylinder (x_1 for the float PTO, x_2 for the paddle PTO). Note that x_2 measures the lengthening and shortening of $\overline{FD}$, which is embedded between the main arm and the paddle arm, so it is a relative coordinate. The coordinates θ_1 and θ_2 are calculated from the coordinates x_1 and x_2. The load cells measure the total forces F_1 and F_2.

Since the motion is periodic, all measured signals are phase-averaged taking the position of the disc $x_1(t)$ as phase reference; in this way the mean oscillation cycle (whose duration is equal to the wave period T) of the measured quantities are derived.

The total dynamic force F' acting on the disc can be calculated by subtracting the static forces (weight and constant part of buoyancy of the stem and the disc) from the total measured force F.

Then, the damping force on the discs F_d can be obtained by subtracting the time-varying buoyancy $-\rho g A_s x$ and the inertia $(m + m_A)\ddot{x}$ from the total dynamic force F':

$$F_d = F' + \rho g A_s x - (m + m_A)\ddot{x} \tag{1}$$

where ρ is the oil density, A_s is the wet section of the stem, m is the total mass of disc and stem, m_A is the added mass of the disc.

If $x(t)$ is periodic and differentiable, the energy E_{12} dissipated by the disc between time instants t_1 and t_2 where disc velocity vanishes is independent on inertia and stiffness forces, and it is:

$$E_{12} = \int_{t1}^{t2} P dt \equiv \int_{t1}^{t2} F_d \dot{x} dt = \int_{t1}^{t2} F' \dot{x} dt \tag{2}$$

where P is the instantaneous power dissipated by the disc. E_{12} represents the mechanical energy extracted by the float or by the paddle from the waves during the time interval included between t_1 and t_2, which can be the instants that subdivide a whole cycle or the ascent and descent phases of the cycle (nominally half-cycle). The disk added mass is equal to $m_A = C_A m_{A0}$, where $m_{A0} = \frac{1}{3} \rho D^3$ is the theoretical added mass for a heaving disc in unbounded flow [23]. The coefficient C_A takes into account the confinements effects; it was calculated using the Fourier analysis, according to [23]:

$$C_A = \frac{1}{\omega X \pi m_{A0}} \int_0^T F'(t) \sin(\omega t) dt \tag{3}$$

where X is the motion amplitude and $\omega = 2\pi/T$ is the motion (and wave) pulsation.

This optimization gave $C_A \approx 2$ for all the discs used. It must be said that the value of C_A does not affect the estimation of the energy dissipated by the disc during the oscillation cycle and during the ascent and descent phases, but only little affects the estimation of instantaneous damping force and dissipated power.

As an example, Figure 4 shows the phase-averaged temporal story of the heaving disc of float PTO. Position x_1, velocity, forces and dissipated power are reported. In order to calculate the equivalent linear damping of the PTOs, we calculated the harmonic approximations $\tilde{\theta}_1(t)$ and $\tilde{\theta}_2(t)$ of the phase-averaged rotations of the main arm $\theta_{1ph}(t)$ and of the paddle arm $\theta_{2ph}(t)$ for each test.

$$\begin{aligned} \tilde{\theta}_1(t) &\equiv \mathrm{Re}\left[\hat{\Theta}_1 e^{i\omega t}\right] \\ \tilde{\theta}_2(t) &\equiv \mathrm{Re}\left[\hat{\Theta}_2 e^{i\omega t}\right] \end{aligned} \tag{4}$$

The complex Fourier coefficients of the first harmonic $\hat{\Theta}_1$ and $\hat{\Theta}_2$ were calculated as (for simplicity in the continuous form):

$$\begin{aligned} \hat{\Theta}_1 &= \tfrac{1}{2T} \int_0^T \theta_{1ph}(t) e^{-i\omega t} dt \\ \hat{\Theta}_2 &= \tfrac{1}{2T} \int_0^T \theta_{2ph}(t) e^{-i\omega t} dt \end{aligned} \tag{5}$$

Then, the equivalent linear torque damping b_{1eq} and b_{2eq} applied to the float and to the paddle are:

$$b_{1eq} \equiv \frac{E_1}{\int_0^T \dot{\tilde{\theta}}_1^2 dt} = \frac{E_1}{\omega \pi \Theta_1^2} \tag{6}$$

$$b_{2eq} \equiv \frac{E_2}{\int_0^T \left(\dot{\tilde{\theta}}_2 - \dot{\tilde{\theta}}_1\right)^2 dt} = \frac{E_2}{\omega \pi \left(\Theta_1^2 + \Theta_2^2 - 2\Theta_1\Theta_2 \cos(\phi_1 - \phi_2)\right)} \tag{7}$$

where Θ_1, Θ_2 are the real amplitudes and ϕ_1, ϕ_2 are the phases, calculated from the complex amplitudes $\hat{\Theta}_1$ and $\hat{\Theta}_2$.

Equation (7) takes into account the rotation of the main arm θ_1 as well, because θ_2 is an absolute coordinate, while paddle damping is embedded between the main arm and the paddle arm. In order to give a more realistic estimation of paddle damping, which was intentionally different in the forward and backward phases, the subsequent expressions were used:

$$b_{2eq,forth} = \frac{E_{2,forth}}{\frac{1}{2} \int_0^T \left(\dot{\tilde{\theta}}_2 - \dot{\tilde{\theta}}_1 \right)^2 dt} \tag{8}$$

$$b_{2eq,back} = \frac{E_{2,back}}{\frac{1}{2} \int_0^T \left(\dot{\tilde{\theta}}_2 - \dot{\tilde{\theta}}_1 \right)^2 dt} \tag{9}$$

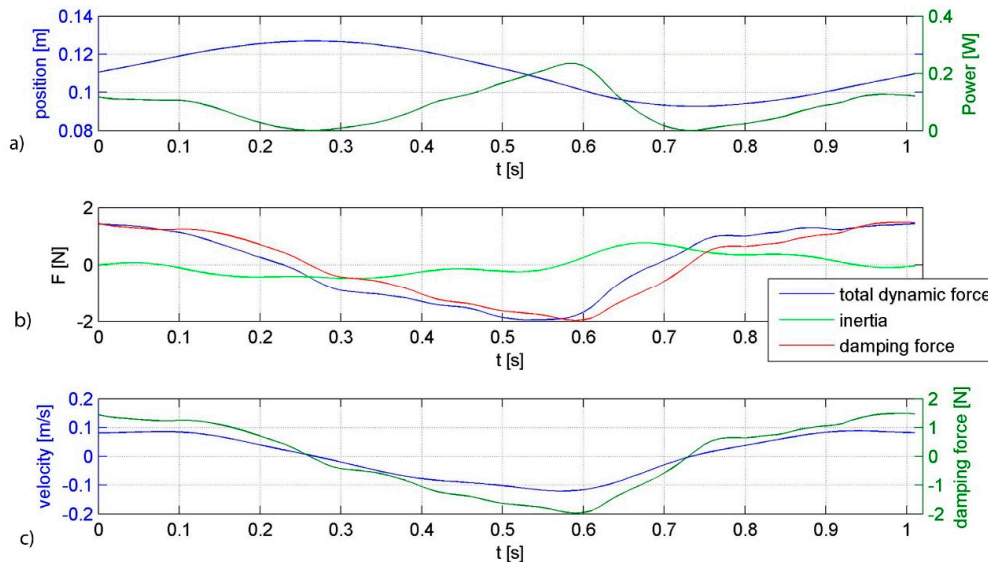where $E_{2,forth}$ and $E_{2,back}$ are the energy dissipated in the forward and backward phases.

Figure 4. Phase averaged oscillation of the heaving disc of the float. $h_F/D = 0.7$, wave A (see Table 2), disc diameter 96 mm. (**a**) Position and dissipated power; (**b**) Forces; (**c**) Velocity and damping force. The total dynamic force in (**b**) is the total measured force minus the static contributions (weight and constant part of buoyancy of the disc and stem).

For the float PTO, four discs of different diameter were used, in order to generate a different amount of damping: depending on the disc diameter, equivalent linear torque damping ranged from 2 to 5 Nms/rad. For the paddle PTO, the same disc configuration was used in all tests. The equivalent linear torque damping generated on the paddle was $b_{2eq,forth} = 0.5$ Nms/rad in the forward phase and $b_{2eq,back} = 0.2$ Nms/rad in the backward phase.

Tests made on the float-only configuration were also useful to quantify the benefits brought by the paddle to the system; to make a reasonable comparison, we decided to set the same mass in the two configurations. System mass is one of the parameters that most affects response motion and CWR; moreover, it is linked to the structure costs. Hence, the inertia moment around O was the same for the float-only system and for the EDS, the latter being calculated considering the second degree of freedom blocked ($\theta_2 = \theta_1$, and paddle arm in vertical position at rest). Moment of inertia I is reported in Table 1. Natural period T_N of the float-only configuration (Table 1) was measured through free oscillations in calm water, by giving an initial displacement to the float and then releasing it.

2.3. Laboratory Waves

The EDS model was tested inside the wave flume of the Hydraulics Laboratory of Politecnico di Milano. The scheme of the wave flume is shown in Figure 5. The flume was 30 m long, 1 m wide, 0.7 m high and it was equipped with a piston wavemaker. A smooth beach with a slope of 7° was placed at the end of the channel. The water depth in the channel was the same for all the tests, $h = 0.4$ m. Wave properties were measured by capacitive wave gauges, without the wave energy converter being in the channel.
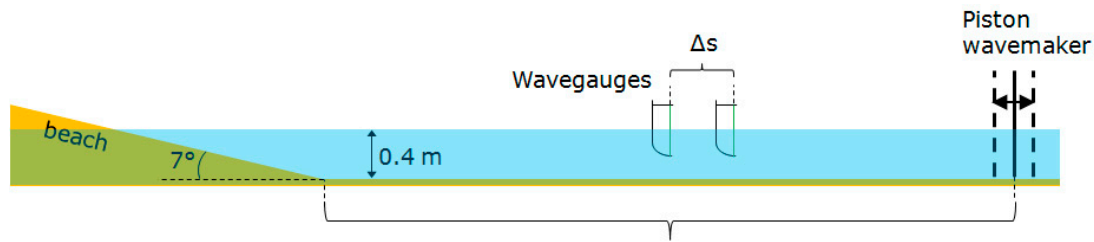
Figure 5. Scheme of the wave flume.

The method of Goda & Suzuki [24] was used to separate the incident and reflected waves. The coefficient of reflection was similar for the three waves considered. Waves properties are reported in Table 2.

Table 2. Laboratory waves.

Wave Type	Incident Wave Amplitude	Reflected Wave Amplitude	Wave Period	Theoretical Wave Length	Experimental Wave Length	Incident Wave Power	Reflection Coefficient
	a_I [mm]	a_R [mm]	T [s]	L_{th} [m]	L_{exp} [m]	P_I[W/m]	r [%]
Wave A	24.4	1.6	1.02	1.52	1.50	2.70	6.4
Wave B	25.4	1.6	1.36	2.29	2.30	3.97	6.2
Wave C	31.7	2.1	1.20	1.92	1.91	5.45	6.8

Wave power per unit crest width was calculated from linear theory (see for example [25]):

$$P_I = \frac{1}{8}\rho g (2a_I)^2 C_g \tag{10}$$

where C_g is the group celerity, calculated according to the water depth in the channel and using the dispersion relation (see for example [25]).

The wave length was also experimentally measured, through cross correlation of the signals of the two wave gauges. In Table 2 the theoretical and experimental values of wave length are reported. Finally, the capture width ratio CWR of EDS was calculated as:

$$\text{CWR} = \frac{P_a}{P_I D} = \frac{\frac{E_1 + E_2}{T}}{P_I D} \tag{11}$$

where P_a is the average power absorbed by the system and $P_I D$ is the wave power of a wave front whose width is equal to the width of the wave energy converter. E_1 and E_2 are the energy absorbed by float and paddle during one oscillation cycle, T is the wave period, D is the float diameter, P_I the wave power for unit crest width calculated on the basis of the incident wave height. For the float-only system $E_2 = 0$.

3. Results

Float-only system was tested first. The system was not in resonance with any of the waves tested, because its natural period was smaller than any wave periods. The water level in the channel was the same for all tests, $h = 0.4$ m. The system was tested at different distances from the shoreline (and hence different depths h_F), and with different values of damping b_1. The position of the system was varied by rigidly moving, along the channel, the structure that supports the WEC model (the points fixed on the structure are the pivot O and the cylinder of the float damping system). In the condition of the maximum proximity of the system to the shore that was tested, water depth at the float was $h_F = 0.12$ m ($h_F/D = 0.6$); this was the limit beyond which the float touched the bottom when oscillating under the wave tested.

Figures 6–8 show the CWR of the float-only system, for the three waves considered (waves A, B, C respectively). The dimensionless water depth h_F/D is reported in the abscissa. The diameter of the circles is proportional to the equivalent linear torque damping applied to the float, whose amount is reported in the legend. For each h_F/D, different values of damping forces were tested, but optimal damping was not reached in any cases. For a given h_F/D, it can be said that optimal damping was approximately reached if the uppermost circle stands over both a smaller and a bigger circle, which means that the damping-CWR trend at that h_F/D shows a relative maximum; thus the distance between the circles at a given h_F/D provides an indication about how damping affects CWR.

It can be seen that maximum CWR meanly increases as water depth increases and it has an oscillating trend. This is reasonable due to the fact that wave reflection from the beach causes the wave height to oscillate along the channel (i.e., [26]). Figure 6 shows that optimal damping for wave A does not vary much with water depth, corresponding often to the small circles, 2–3 Nms/rad. For wave B and C (Figures 7 and 8), the dimension of the uppermost circles (that indicates the optimal damping) seems to fairly vary with depth, but it is misleading: due to the fact that the same range of float damping was utilized for the three waves, CWR variability with respect to damping is smaller as T/T_N increases, where T is the wave period. The mean optimal damping for the three waves, obtained by averaging the optimal damping at each h_F/D, is $b_{1eq,opt}$ = 2.51, 3.41, 3.16 Nms/rad, respectively for waves A, B, C; this agrees with the periods of the waves, since a higher optimal damping corresponds to a higher wave period, as long as $T/T_N > 1$. Indeed, optimal damping should have a minimum and CWR should have a maximum for $T/T_N = 1$; according to this fact, CWR of the system with wave A is on average higher than CWR with the other two waves, on the contrary there is not much difference between CWR with wave B and C.
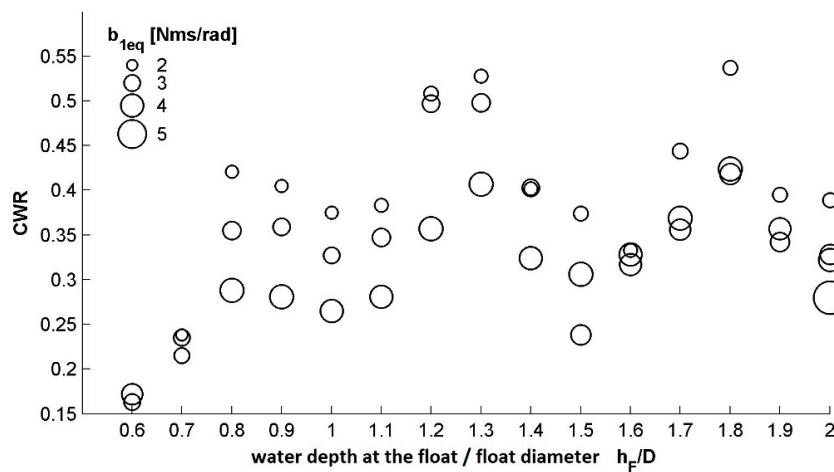

Figure 6. CWR of the float-only system as a function of float damping b_{1eq}, water depth at the float h_F/D. Wave A.
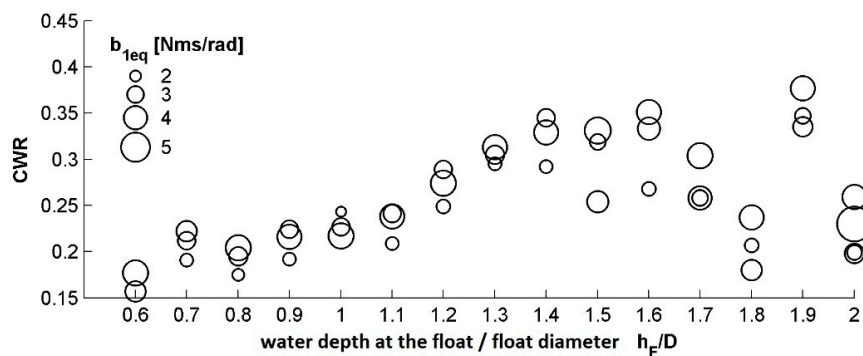

Figure 7. CWR of the float-only system as a function of float damping b_{1eq}, water depth at the float h_F/D. Wave B.
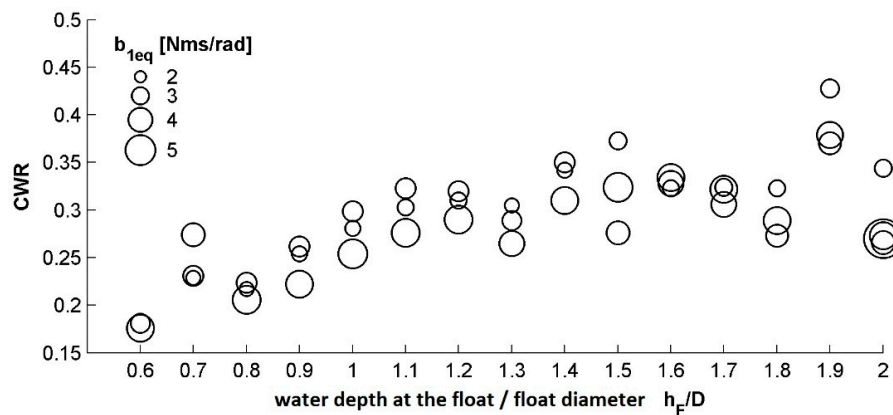
Figure 8. CWR of the float-only system as a function of float damping b_{1eq}, water depth at the float h_F/D. Wave C.

Figure 6 shows that the highest CWR almost always occurs with the minimum damping applied. However, it was not possible to reach the optimal damping for wave A due to the physical limitation of PTO amplitude and the necessity to avoid the float touching the channel bottom when h_F/D was low. Again in Figure 6, for low depths $h_F/D = 0.6$ and $h_F/D = 0.7$, the applied damping does not significantly affect the CWR of the float. This fact is less evident for waves B and C in Figures 7 and 8.

Then, the complete EDS system was tested. Different distances between paddle and float d_{P-F}, water depth at the float h_F and float external damping b_{1eq} were varied in the tests. The configuration of paddle PTO was the same for all the tests: two discs inside the cylinder were used in order to generate asymmetric damping. Due to the great number of parameters that characterizes the EDS system, only some of them have been optimized in this work, while other ones, like paddle damping, will be investigated in future works. The paddle immersion at rest was $d_P = 0.09$ m in all the tests; this value was found to be optimal in the previous work [21].

Figures 9–11 show CWR of the EDS system for the three waves A, B, C. Not all the combinations of the three parameters (h_F/D, b_{1eq}, d_{P-F}) are reported: we have neglected the configurations that were clearly less efficient. For each wave, float optimal damping of the EDS is similar to the one of the float-only system: averaging the best configurations for each h_F/D, we obtain $b_{1eq,opt} = 2.17$, 3.77, 3.15 Nms/rad for waves A, B, C. This result suggests that float optimal damping is independent from the presence of the paddle.
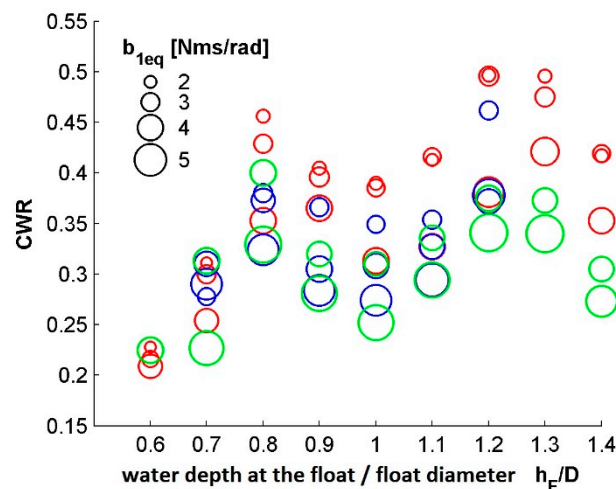

Figure 9. CWR of EDS as a function of flat damping b_{1eq}, distance between paddle and float d_{P-F}/D, water depth at the float h_F/D. Red circles, $d_{P-F}/D = 0.8$; blue circles, $d_{P-F}/D = 1.1$; green circles $d_{P-F}/D = 1.4$. Wave A.
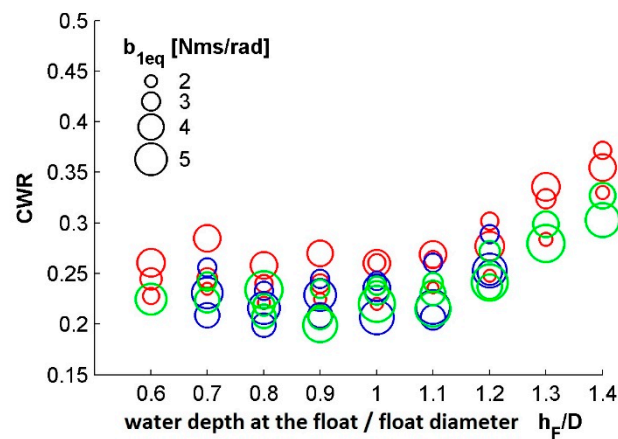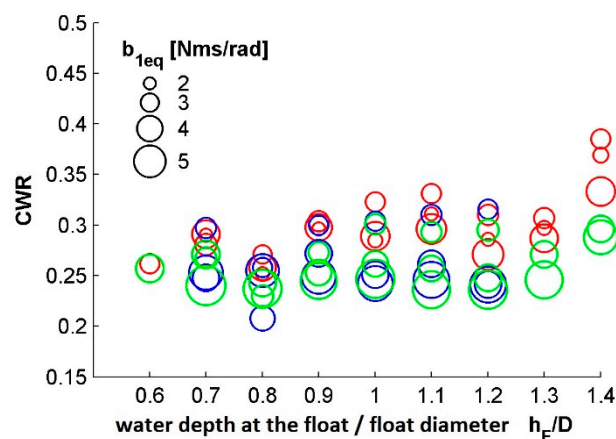
Figure 10. CWR of EDS as a function of flat damping b_{1eq}, distance between paddle and float $d_{P\text{-}F}/D$, water depth at the float h_F/D. Red circles, $d_{P\text{-}F}/D$ = 0.8; blue circles, $d_{P\text{-}F}/D$ = 1.1; green circles $d_{P\text{-}F}/D$ = 1.4. Wave B.

Figure 11. CWR of EDS as a function of flat damping b_{1eq}, distance between paddle and float $d_{P\text{-}F}/D$, water depth at the float h_F/D. Red circles, $d_{P\text{-}F}/D$ = 0.8; blue circles, $d_{P\text{-}F}/D$ = 1.1; green circles $d_{P\text{-}F}/D$ = 1.4. Wave C.

The best configuration of EDS is almost always the one with $d_{P\text{-}F}/D$ = 0.8, for all the three waves. There is no appreciable difference between the configurations with $d_{P\text{-}F}/D$ = 1.1 and $d_{P\text{-}F}/D$ = 1.4. Like the float-only configuration, the EDS CWR meanly increases as water depth increases and it oscillates. Again, for water depth h_F/D < 0.8, CWR is less sensitive to damping.

These tests revealed that the performance of EDS have been improved with respect to the previous model [21]: although the system inertia has been significantly decreased in order to make the model more realistic (less weight, smaller size), CWR on wave A and C are similar or higher than the ones found in [21]. This is due to the improvements in structure and mechanics made on the EDS model, which include a better bearings system and a more realistic paddle PTO, which in the model in [21] simply consisted of a spring.

4. Discussion

In Figure 12 the results obtained with the float-only system are compared with the ones of [22], in which a scale model of a similar WEC, the Wavestar, was tested. CWR against dimensionless wave frequency $\omega^2 r_0/g$ is reported, for different values of wave steepness *H/L*. r_0 is the radius of the wet perimeter of the float at rest. The present results are shown in terms of mean *CWR* $\pm$ standard deviation along the beach, for a given wave frequency. The results of [22] are obtained in random waves, with ω being the wave peak pulsation. It must be said that, for a given $\omega^2 r_0/g$, our system has

a slightly smaller T/T_N than the one of [22]: this could bring a higher CWR for our float. Though it is difficult to make a precise comparison, the present results of CWR are comparable with the ones found by [22].

In Figure 13 optimal damping of the float-only system is compared with the one found by [22]. Again, our results are presented in terms of mean optimal damping $\pm$ standard deviation along the beach for a given wave frequency. The dimensionless optimal damping was calculated as $b_{ext}/(\rho V_0 \omega l_1)$, where V_0 is the immersed volume of the float at rest and l_1 is the float arm ($\overline{OA}$ in our system). Present results agree with the ones of [22] except for wave A. This disagreement could be caused by the fact that we could not further decrease float damping and reach the optimal value due to the physical constraints of the model.
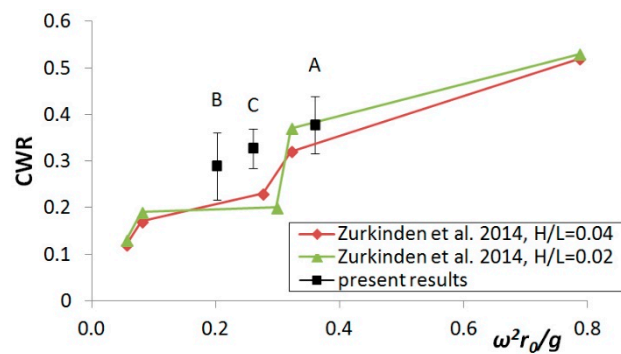
Figure 12. CWR as a function of wave dimensionless frequency. Wave A: $H/L = 0.03$; wave B: $H/L = 0.02$; wave C: $H/L = 0.03$.
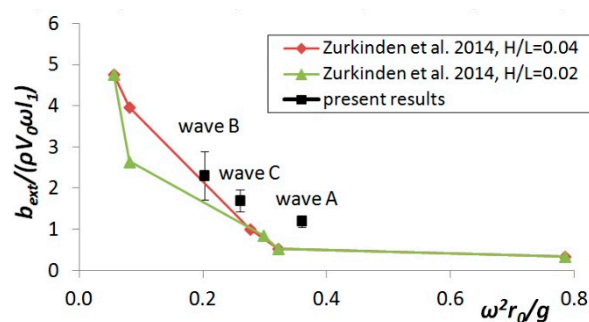

Figure 13. Dimensionless optimal damping for the float-only configuration. Wave A: $H/L = 0.03$; wave B: $H/L = 0.02$; wave C: $H/L = 0.03$.

For each wave, the best configuration of EDS was compared with the best configuration reached with the float-only system (Figure 14). On average, CWR of EDS is 5% (in absolute) higher than the one of the float-only system; relatively speaking, the CWR of the system can increase, with the addition of the paddle, by 10÷50% for $h_F/D \leq 0.8$. This advantage tends to decrease as h_F/D increases. This is due to the fact that, increasing depth, the horizontal wave force decreases and the energy captured by the paddle decreases. For $h_F/D < 0.8$, CWR of EDS is up to 1.5 times CWR of the float-only system.

Figures 15–17 show how CWR of EDS is distributed among float and paddle, for the best configuration of EDS and float-only system, for low h_F/D; furthermore, energy is split into the upward and downward phases of the float and forward and backward phases for the paddle.
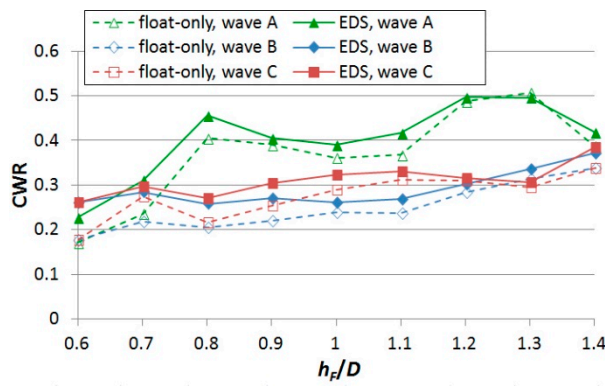
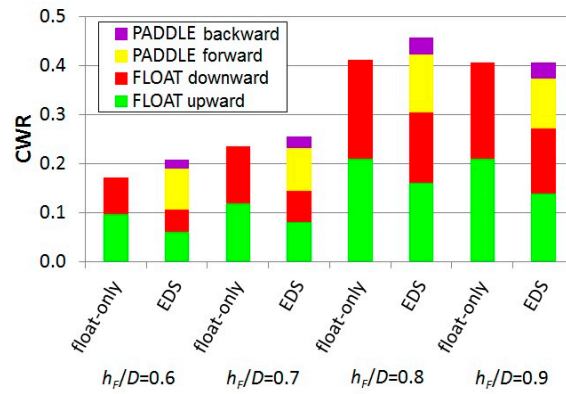**Figure 14.** Comparison between CWR of EDS and float -only system at best configuration.

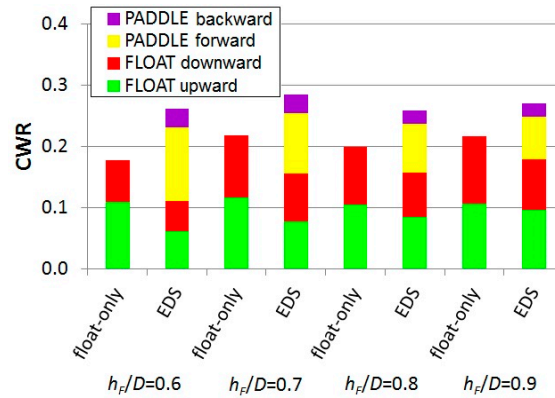**Figure 15.** CWR distribution among float and paddle, and motion phases of each body. Wave A.

Figure 16. CWR distribution among float and paddle, and motion phases of each body. Wave B.
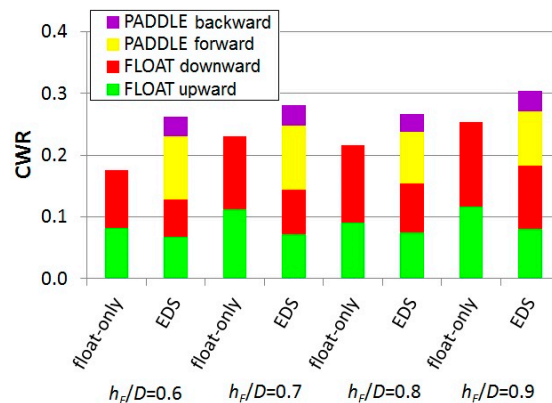

Figure 17. CWR distribution among float and paddle, and motion phases of each body. Wave C.

The charts show that the energy absorbed by the paddle in the forward phase is much higher than in the backward phase, because of the asymmetrical external damping and of the mass transport of the waves in shallow water. For $h_F/D \leq 0.9$, the CWR of the paddle is 10–15%, with about 10% in the forward phase, which is higher than the 5% found in reference [20] for a surging paddle pushed by the waves in deep water; this is likely due to the fact that the surge wave force is higher in shallow water than in deep water. On the contrary, the surging flap tested in reference [15] showed a CWR significantly higher (>20%) than the EDS paddle, probably due to the fact that, in reference [15], the damping applied to the flap was optimized.

CWR of the float in the upward and downward phase tends to be equal as water depth increases, due the reduction of wave nonlinearity. As seen before, the presence of the paddle increases the total CWR of EDS, though generally decreases the float CWR, with respect to the case of the float-only system.

5. Conclusions

The behavior of two oscillating-body WECs on a sloping bottom has been investigated: a pitching-heaving float and the EDS, an innovative multibody WEC composed by the pitching-heaving float and a pitching-surging paddle.

The position of the WEC was found to be very influential on its performance. This is imputable to the properties of the waves, which change as water depth changes, and to the wave reflection from the sloping bottom: a high variation of CWR with the position of the WEC is observed. On average, CWR of the WEC increases as water depth increases, but presents significant oscillation due to the wave height oscillation along the wave propagation direction. This is very important in order to localize optimal positions for a nearshore WEC.

The main parameters that characterize EDS have been investigated, and indications about its optimal configuration have been found. EDS performances were compared with the ones of the float-only system with the same inertia, and the results obtained show that EDS almost always has a higher CWR. This is even more interesting, considering that the implementation of a paddle on a system with a heaving float does not require significant changes in the supporting structure. Optimal damping of the float is generally independent from water depth, except for water depth $h_F/D < 0.8$, where a wider range of damping brings a similar power production. This is valid both for the float-only system and for the EDS: for a given system mass, optimal float damping for the float-only system and the EDS is similar.

For the water depths tested $h_F/D = 0.6$–1.4, EDS is more efficient than the float-only system, more significantly in water depth $h_F/D = 0.6$, where the CWR of EDS is about 1.5 times the CWR of the float-only system. EDS advantage on the float-only system decreases as water depth increases, although it is still present, at least up to $h_F/D = 1.4$. The EDS advantage on the float-only system is due to the fact that the energy contribution of the paddle exceeds the energy decrease of the float when inside the EDS system.

These results confirm that EDS is particularly interesting for shallow water, and, thanks to its structure, it is particularly suited to be docked on the external side of breakwaters of ports.

The distance between paddle and float also affects the CWR of EDS: best results were obtained with the paddle close to the float.

The results obtained on EDS are encouraging, also because the system still has room for improvement. In our opinion, the optimization of paddle damping in particular may further increase the CWR of EDS.

Author Contributions: M.N. contributed in designing and developing the experimental setup, designing and realizing the experiments, analyzing the results and writing the paper. S.M. supervised the research and contributed in designing the experimental setup and the experiments and writing the paper.

References

1. de O Falcao, A.F. Wave energy utilization: A review of the technologies. *Renew. Sustain. Energy Rev.* **2010**, *14*, 899–918. [CrossRef]

2. López, I.; Andreu, J.; Ceballos, S.; Martinez de Alegría, I.; Kortabarria, I. Review of wave energy technologies and the necessary power-equipment. *Renew. Sustain. Energy Rev.* **2013**, *27*, 413–434. [CrossRef]

3. Khan, N.; Kalair, A.; Abas, N.; Haider, A. Review of ocean tidal, wave and thermal energy technologies. *Renew. Sustain. Energy Rev.* **2017**, *72*, 590–604. [CrossRef]

4. Perez-Collazo, C.; Greaves, D.; Iglesias, G. A Novel Hybrid Wind-Wave Energy Converter for Jacket-Frame Substructures. *Energies* **2018**, *11*, 637. [CrossRef]

5. Fadaeenejad, M.; Shamsipour, R.; Rokni, S.D.; Gomes, C. New approaches in harnessing wave energy: With special attention to small islands. *Renew. Sustain. Energy Rev.* **2014**, *29*, 345–354. [CrossRef]

6. Roy, A.; Auger, F.; Dupriez-Robin, F.; Bourget, S.; Tran, Q.T. Electrical Power Supply of Remote Maritime Areas: A Review of Hybrid Systems Based on Marine Renewable Energies. *Energies* **2018**, *11*, 1904. [CrossRef]

7. Folley, M.; Whittaker, T.J.T. Analysis of the nearshore wave energy resource. *Renew. Energy* **2009**, *34*, 1709–1715. [CrossRef]

8. Van Nieuwkoop-McCall, J.C.C.; Smith, H.C.M.; Edwards, K.A. Effect of water depth on the wave energy resource and extreme wave conditions. In Proceedings of the 4th International Conference on Ocean Energy (ICOE 2012), Dublin, Ireland, 17–19 October 2012.

9. Vicinanza, D.; Contestabile, P.; Ferrante, V. Wave energy potential in the north-west of Sardinia (Italy). *Renew. Energy* **2013**, *50*, 506–521. [CrossRef]

10. Morim, J.; Cartwright, N.; Etemad-Shahidi, A.; Strauss, D.; Hemer, M. A review of wave energy estimates for nearshore shelf waters off Australia. *Int. J. Mar. Energy* **2014**, *7*, 57–70. [CrossRef]

11. Rusu, E.; Guedes Soares, C. Numerical modelling to estimate the spatial distribution of the wave energy in the Portuguese nearshore. *Renew. Energy* **2009**, *34*, 1501–1516. [CrossRef]

12. Purandare, M.M.; Aswatha Narayana, P.A. Wave power variation in the near-shore regions. *Coast. Eng.* **1987**, *11*, 381–390. [CrossRef]

13. Belibassakis, K.; Bonovas, M.; Rusu, E. A Novel Method for Estimating Wave Energy Converter Performance in Variable Bathymetry Regions and Applications. *Energies* **2018**, *11*, 2092. [CrossRef]

14. Silva, D.; Rusu, E.; Guedes-Soares, C. Evaluation of Various Technologies for Wave Energy Conversion in the Portuguese Nearshore. *Energies* **2018**, *6*, 1344. [CrossRef]

15. Folley, M.; Whittaker, T.J.T.; Henry, A. The effect of water depth on the performance of a small surging wave energy converter. *Ocean Eng.* **2007**, *34*, 1265–1274. [CrossRef]

16. Whittaker, T.J.T.; Folley, M. Nearshore oscillating wave surge converters and the development of Oyster. *Philos. Trans. R. Soc. A* **2012**, *370*, 345–364. [CrossRef] [PubMed]

17. Hansen, R.H.; Kramer, M.M.; Vidal, E. Discrete Displacement Hydraulic Power Take-Off System for the Wavestar Wave Energy Converter. *Energies* **2013**, *6*, 4001–4044. [CrossRef]

18. Falcão, A.F.O.; Cândido, J.J.; Justino, P.A.P.; Henriques, J.C.C. Hydrodynamics of the IPS buoy wave energy converter including the effect of non-uniform acceleration tube cross section. *Renew. Energy* **2012**, *41*, 105–114. [CrossRef]

19. Muliawan, M.J.; Gao, Z.; Moan, T.; Babarit, A. Analysis of a Two-Body Floating Wave Energy Converter with Particular Focus on the Effects of Power Take-Off and Mooring Systems on Energy Capture. *J. Offshore Mech. Arct. Eng.* **2013**, *135*. [CrossRef]

20. Hazlett, B.D.; Inculet, I.I.; Inculet, D.R. Electric power generation by "surfing" water waves. *Renew. Energy* **2009**, *34*, 2510–2514. [CrossRef]

21. Negri, M.; Clerici, F.; Malavasi, S. A breaker-zone wave energy converter. In Proceedings of the International Conference on Renewable Energies and Power Quality (ICREPQ'13), Bilbao, Spain, 20–22 March 2013.

22. Zurkinder, A.S.; Ferri, F.; Beatty, S.; Kofoed, J.P.; Kramer, M.M. Non-linear numerical modelling and experimental testing of a point absorber wave energy converter. *Ocean Eng.* **2014**, *78*, 11–21. [CrossRef]

23. Sarpkaya, T.; Isaacson, M. Mechanics of wave forces on offshore structures. *J. Appl. Mech.* **2009**, *49*, 466–467. [CrossRef]

24. Goda, Y.; Suzuki, Y. Estimation of incident and reflected waves in random wave experiments. In Proceedings of the 15th Coastal Engineering Conference, Honolulu, HI, USA, 1–17 July 1976.

25. Dean, R.G.; Dalrymple, A.R. *Water Wave Mechanics for Engineers and Scientists*; World Scientific Publishing Co. Pte. Ltd.: Singapore, 1991; p. 370, ISBN 978-9810204211. Available online: https://books.google.com.hk/books?hl=zh-TW&lr=&id=1SM8DQAAQBAJ&oi=fnd&pg=PR7&dq=Water+Wave+Mechanics+for+Engineers+and+Scientists&ots=H6H52F2eUF&sig=vV45k69GgImGHVmN6V3TmRfLKN0&redir_esc=y#v=onepage&q=Water%20Wave%20Mechanics%20for%20Engineers%20and%20Scientists&f=false (accessed on 24 July 2018).

26. Chang, H.-K.; Hsu, T.-W. A two-point method for estimating wave reflection over a sloping beach. *Ocean Eng.* **2003**, *30*, 1833–1847. [CrossRef]